



**HAL**  
open science

# Dynamic and thermodynamic crossover scenarios in the Kob-Andersen mixture: Insights from multi-CPU and multi-GPU simulations

Daniele Coslovich, Misaki Ozawa, Walter Kob

► **To cite this version:**

Daniele Coslovich, Misaki Ozawa, Walter Kob. Dynamic and thermodynamic crossover scenarios in the Kob-Andersen mixture: Insights from multi-CPU and multi-GPU simulations. *European Physical Journal E: Soft matter and biological physics*, 2018, 41 (5), pp.62. 10.1140/epje/i2018-11671-2 . hal-01818216

**HAL Id: hal-01818216**

**<https://hal.science/hal-01818216>**

Submitted on 11 Jan 2024

**HAL** is a multi-disciplinary open access archive for the deposit and dissemination of scientific research documents, whether they are published or not. The documents may come from teaching and research institutions in France or abroad, or from public or private research centers.

L'archive ouverte pluridisciplinaire **HAL**, est destinée au dépôt et à la diffusion de documents scientifiques de niveau recherche, publiés ou non, émanant des établissements d'enseignement et de recherche français ou étrangers, des laboratoires publics ou privés.

# Dynamic and thermodynamic crossover scenarios in the Kob-Andersen mixture: Insights from multi-CPU and multi-GPU simulations

Daniele Coslovich,<sup>1</sup> Misaki Ozawa,<sup>1</sup> and Walter Kob<sup>1</sup>

*Laboratoire Charles Coulomb, Université de Montpellier, CNRS, Montpellier, France*

The physical behavior of glass-forming liquids presents complex features of both dynamic and thermodynamic nature. Some studies indicate the presence of thermodynamic anomalies and of crossovers in the dynamic properties, but their origin and degree of universality is difficult to assess. Moreover, conventional simulations are barely able to cover the range of temperatures at which these crossovers usually occur. To address these issues, we simulate the Kob-Andersen Lennard-Jones mixture using efficient protocols based on multi-CPU and multi-GPU parallel tempering. Our setup enables us to probe the thermodynamics and dynamics of the liquid at equilibrium well below the critical temperature of mode-coupling theory,  $T_{\text{MCT}} = 0.435$ . We find that below  $T = 0.4$  the analysis is hampered by partial crystallization of the metastable liquid, which nucleates extended regions populated by large particles arranged in an fcc structure. By filtering out crystalline samples, we reveal that the specific heat grows in a regular manner down to  $T = 0.38$ . Possible thermodynamic anomalies suggested by previous studies can thus occur only in a region of the phase diagram where the system is highly metastable. Using the equilibrium configurations obtained from the parallel tempering simulations, we perform molecular dynamics and Monte Carlo simulations to probe the equilibrium dynamics down to  $T = 0.4$ . A temperature-derivative analysis of the relaxation time and diffusion data allows us to assess different dynamic scenarios around  $T_{\text{MCT}}$ . Hints of a dynamic crossover come from analysis of the four-point dynamic susceptibility. Finally, we discuss possible future numerical strategies to clarify the nature of crossover phenomena in glass-forming liquids.

## I. INTRODUCTION

If a liquid is cooled quickly enough, it will bypass crystallization and form an amorphous solid called glass. Such a glass transition is directly related to the rapid increase of the structural relaxation time upon cooling, whose temperature-dependence is given by the Arrhenius law for strong glass-formers and is super-Arrhenius for fragile glass-formers<sup>1</sup>. Despite being purely kinetic in nature, the glass transition is accompanied by a change in the thermodynamic properties of the system at the glass transition temperature  $T_g$ . For instance, the specific heat shows a mild increase upon cooling and displays a drop at  $T_g$  due to the freezing of the configurational degrees of freedom. Although no phase transition occurs at  $T_g$ , it has been suggested that the slowing down of the dynamics and the resulting glass formation might be driven by a hidden phase transition<sup>2,3</sup>.

While most glass-forming liquids follow the trends outlined above, there are notable exceptions. This is the case for instance of liquids with strong, directional interactions, such as silica, silicon, and water. These systems display a thermodynamic anomaly in the form of a local maximum of the specific heat at a temperature  $T^* > T_g$ <sup>4</sup>, a behavior which has also been observed in simulation studies of silica<sup>5,6</sup>, supercooled water<sup>7</sup>, and other simple models<sup>8–11</sup>. Concomitantly, also the dynamic behavior of these liquids changes around  $T^*$ , crossing over from a super-Arrhenius to an Arrhenius temperature dependence (“fragile-to-strong” crossover). The origin of these thermodynamic and dynamic anomalies has often been attributed to the presence, or proximity, of a liquid-liquid transition or its Widom-line, located at

temperatures higher than  $T_g$ <sup>4</sup>. Interestingly, this fragile-to-strong crossover is not limited to systems with directional interactions<sup>12</sup>. Recent experimental<sup>13,14</sup> and simulational<sup>15</sup> studies have demonstrated that also several metallic glass-formers exhibit a notable fragile-to-strong crossover. Several interpretations have been proposed to explain the crossover in these systems, including the presence of thermodynamic anomalies such as a liquid-liquid transition<sup>15–17</sup>, anomalous crystallization<sup>18</sup>, or the evolution of structural medium range order<sup>14</sup>.

The dynamics of some molecular and polymeric liquids show even a different kind of crossover at a temperature  $T_D$ , typically located about 15%-25% above  $T_g$ . This dynamic crossover thus occurs when the relaxation times are around  $10^{-8} - 10^{-6}$  s and is subtle, but it can be revealed by temperature-derivative analysis of high-quality dynamic measurements in molecular glass-formers<sup>19–21</sup>. At  $T_D$  the increase of relaxation times crosses over from super-Arrhenius to a milder temperature dependence and tend to become Arrhenius at very low temperature. While some authors have considered systems with such a crossover as marginal cases<sup>22</sup>, an alternative point of view suggests that this behavior may be fairly general<sup>12</sup>, even though the location of the crossover is highly system-dependent<sup>20,21</sup>.

The physical origin of this dynamic crossover is not completely clear and there are diverging viewpoints on this. Some authors have pointed out the closeness of  $T_D$  with the temperature at which a power law fit predicts a divergence of the relaxation time data<sup>12,23,24</sup>. The dynamic crossover should then be identified with the critical temperature of mode-coupling theory (MCT)<sup>25</sup>. Others have attributed this crossover to an upper limit of the

activation energy<sup>21,22</sup>, which may saturate at an arbitrarily low temperature. While these two interpretations are completely different in nature, they are difficult to disentangle in practice. We emphasize that the dynamic crossover scenario is a priori unrelated from one that accompanies liquid-liquid transitions, in that the former does not involve the thermodynamics and is purely dynamic in origin.

Also computer simulations have been used to probe the existence of anomalies in the dynamic and thermodynamic properties of glass-forming liquids. The results of these studies suggest that both the dynamic correlation length scales<sup>26</sup> and the dynamic finite size effects<sup>27</sup> may show a crossover compatible with several theoretical predictions<sup>28–30</sup>, although these results do not seem to hold universally. On the other hand, the dynamic range accessible in conventional numerical studies is limited to only 4-5 decades in time. Thus, some of these results might be affected by insufficient equilibration.

In the present study, we focus on a simple glass-former, proposed by Kob and Andersen (KA)<sup>31</sup>, that has so far been fairly robust against crystallization and hence has been used in many investigations of the glass-transition. Previous studies of this system have given evidence for the presence of a thermodynamic anomaly in the form of a peak in the specific heat<sup>32</sup> and a possible fragile-to-strong crossover<sup>33,34</sup>, although these results might have been affected by finite size and finite sampling effects. In the present work we employ an optimized simulation setup, which exploits the parallel tempering method<sup>35</sup> and state-of-art molecular dynamics code running on graphics processing units (GPU), to extend the temperature range in which thermodynamic and dynamic measurements can be done at equilibrium. We find that, in contrast to previous reports<sup>32</sup>, the thermodynamics of the liquid is regular. At lower temperatures, simulations are hindered by crystallization, which involves structures of fcc symmetry formed by large particle. Finally, we discuss possible ways and setups to detect numerically the presence of dynamic anomalies in model glass-formers.

## II. MODEL AND METHODS

### A. Model parameters

The system we consider is a binary mixture in which both species have the same mass  $m$ . The particles interact via a Lennard-Jones potential given by

$$u_{\alpha\beta}(r) = 4\epsilon_{\alpha\beta} \left[ \left( \frac{\sigma_{\alpha\beta}}{r} \right)^{12} - \left( \frac{\sigma_{\alpha\beta}}{r} \right)^6 \right], \quad (1)$$

where  $\alpha, \beta \in \{A, B\}$  are species indices. The value of the parameters  $\sigma_{\alpha\beta}$  and  $\epsilon_{\alpha\beta}$  are given in Ref.<sup>31</sup>. The units of length and energy are set by the parameters  $\sigma_{AA} = 1$  and  $\epsilon_{AA} = 1$ , respectively. The potentials are cut and shifted at a distance  $2.5\sigma_{\alpha\beta}$ . We simulate systems com-

posed by  $N$  particles in a cubic box of side  $L$  with periodic boundary conditions and a number density given by  $\rho = N/V = 1.1998$ . Note that even small differences in density can quantitatively affect the thermodynamic and dynamic observables. For example, in the original paper<sup>31</sup> a different density  $\rho = 1.204$  was used, which leads to slight differences in statics and dynamics when sufficiently high quality data are available. The system size ranges from  $N = 300$  to 3600 for parallel tempering simulations (see below). Additional dynamic data have been obtained for a much bigger sample ( $N = 100000$ ) using the LAMMPS simulation package<sup>36,37</sup>.

### B. Simulation protocols

Our simulations implement the parallel tempering (PT) algorithm<sup>35,38</sup>, in which  $M$  replicas of the system of interest perform independently simulations at temperatures  $\{T_i\}$  with the potential energies  $\{U_i\}$ . At regular intervals, exchanges are attempted between pairs of replicas at neighboring states and the temperatures are exchanged with probability

$$p = \min \{1, \exp [(U_i - U_j) (\beta_i - \beta_j)]\}, \quad (2)$$

where  $\beta_i = 1/k_B T_i$  (with  $k_B = 1$  in this study), to ensure detailed balance. Since our simulations extend to a temperature range that remained so far largely unexplored, we used different simulation protocols and software to check and validate our results. Namely, we used two independent implementations of the PT algorithm, each one relying on a different molecular dynamics code to carry out the simulation. Note that, for a given system size, we used the same sets of temperatures for all the PT protocols, namely 0.3730, 0.3810, 0.3901, 0.4003, 0.4115, 0.4238, 0.4374, 0.4525, 0.4692, 0.4877, 0.5082, 0.5307 for  $N = 1200$  and 0.4000, 0.4060, 0.4130, 0.4210, 0.4301, 0.4403, 0.4515, 0.4638, 0.4768, 0.4906 for  $N = 3600$ .

In the first implementation, named **PT-1 protocol**, we perform multi-CPU parallel tempering simulations with an in-house molecular dynamics code. The MD simulations are performed in the  $NVT$  ensemble using the Nose-Hoover thermostat<sup>39</sup> with a time step  $\delta t = 0.004$  and a thermostat relaxation time  $0.4 = 100\delta t$ . We used  $M = 12 - 14$  replicas depending on system size. The code is parallelized using MPI to handle communications between replicas, which attempt to exchange their state, i.e., the temperature of the associated thermostat, every 50000 MD steps.

The second implementation, named **PT-2 protocol**, relies on a multi-GPU parallel tempering code<sup>40</sup> that uses the RUMD package<sup>41</sup> as a simulation backend. This multi-GPU code was implemented in python building on the `atooms` framework<sup>42</sup>. Multiple replicas are simulated on individual GPUs and communication between GPUs are handled at high-level via the `mpi4py` package<sup>43</sup>. We ran the multi-GPU simulations on a dedicated cluster

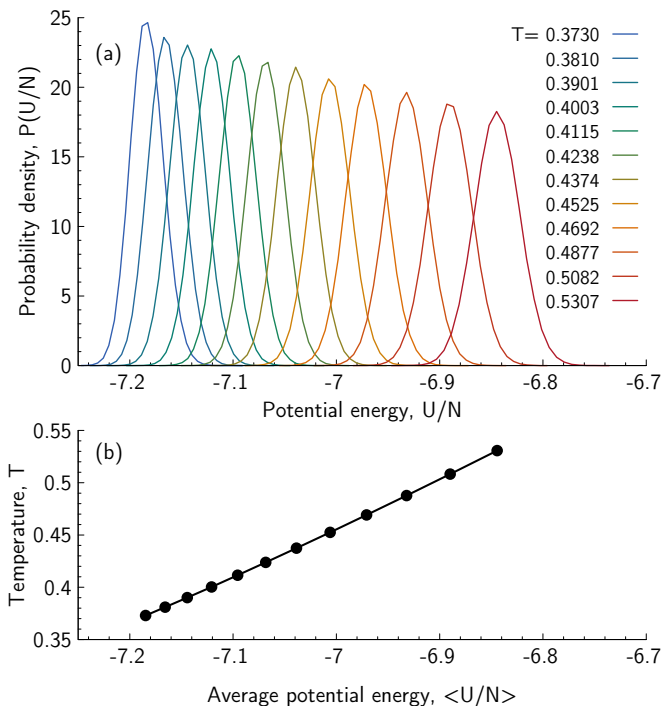


FIG. 1. (a) Distribution of the potential energy per particle  $P(U/N)$  for  $N = 1200$  obtained from the parallel tempering protocol PT-3. Runs with a substantial fraction of crystalline configurations were discarded from the analysis. (b) Average potential energies per particle for each of the studied temperatures.

of inexpensive gaming cards (GTX-980 and even GTX-750Ti). The thermostat is again of the Nose-Hoover type, the time step is  $\delta t = 0.004$  and the thermostat relaxation time  $\tau_T = 0.2 = 50\delta t$ . We used the same exchange intervals and number of replicas as in PT-1. We checked that increasing the interval between exchanges did not change our results.

Finally, we performed additional PT simulations (**PT-3 protocol**) to extend our thermodynamic measurements to even lower temperatures than the ones attained by protocols PT-1 and PT-2. The PT-3 simulations are performed using the multi-GPU code described above starting from uncorrelated configurations obtained using the PT-2 protocol at a temperature  $T = 0.4$ . These efficient multi-GPU simulations enabled us to carefully measure the waiting time dependence of the results so as to assess equilibration issues, see Sec. III A.

From these PT simulations, we evaluated the specific heat per particle  $c_V$  from the fluctuations of the potential energy  $U$ ,

$$c_V = \frac{1}{NT^2} (\langle U^2 \rangle - \langle U \rangle^2) + \frac{3}{2}, \quad (3)$$

and from the temperature derivative of the average potential energy,

$$c_V = \frac{1}{N} \frac{\partial \langle U \rangle}{\partial T} + \frac{3}{2}, \quad (4)$$

where  $\langle (\dots) \rangle$  is the thermal average. The two expressions yield identical results provided the averages are carried out over the equilibrium measure. In a simulation, the agreement between the estimates of  $c_V$  obtained through the two methods is often taken as a test of equilibration. We note that, in practice, only very accurate measurements can reveal discrepancies between the two methods. The distributions  $P(U/N)$  and the  $T$ -dependence of  $\langle U \rangle$  obtained from well-equilibrated simulations (PT-3 protocol) are shown in Fig. 1.

Strictly speaking, parallel tempering simulations only give access to thermodynamic and static properties. However, it is possible to perform extended dynamic measurements by starting “regular” simulations from configurations sampled during the PT simulations at a given temperature. Here, again, we follow two distinct protocols to corroborate our results.

In the **MC protocol** we performed normal Monte Carlo simulations using an in-house code and starting from uncorrelated configurations obtained from protocol PT-1. The MC simulations are carried out in the  $NVT$  ensemble using simple displacement moves<sup>44</sup>, in which we attempt to displace a randomly selected particles over a cube of side 0.15. We used 10 – 30 independent configurations depending on temperature. The length of the simulations at the lowest temperature ( $T = 0.4$ ) is  $10^9$  Monte Carlo steps. In the following, the time unit for the MC protocol is given by one MC sweep, i.e.,  $N$  attempted displacement moves.

In the **MD protocol** we performed molecular dynamics simulations using the RUMD package starting from uncorrelated configurations obtained from protocol PT-1 and PT-2. The MD simulations are carried out in the  $NVT$  ensemble using the Nose-Hoover thermostat, the time step is  $\delta t = 0.004$  and the thermostat relaxation time  $\tau_T = 0.2 = 50\delta t$ . For the  $N = 1200$  samples, we used 128 independent configurations down to  $T = 0.4$  from protocol PT-2. For  $T = 0.39$ , we used only 30 configurations, namely the final configurations of the PT-2 runs. For the  $N = 3600$  samples, we used 20 independent configurations from protocol PT-1. The duration of each of the MD simulations ranged from  $4.2 \times 10^6$  steps (at  $T = 0.51$ ) to  $2.1 \times 10^9$  steps (at  $T = 0.39$ ), thus each run was about 10 – 20 times longer than the typical structural relaxation time  $\tau_\alpha$  (see below for its definition). In total, for each temperature, our simulations cover over about 2500 structural relaxation times. This high-quality statistics enables us to perform a temperature-derivative analysis of the dynamic data, see Sec. III B.

For both MC and MD protocols, we checked that the initial configurations were uncorrelated from one another by measuring their mutual self overlaps<sup>45</sup>

$$Q_s = \frac{1}{N} \sum_i \Theta(a - |\mathbf{r}_i^\alpha - \mathbf{r}_i^\beta|), \quad (5)$$

where  $\alpha$  and  $\beta$  denote two configurations, and their mu-

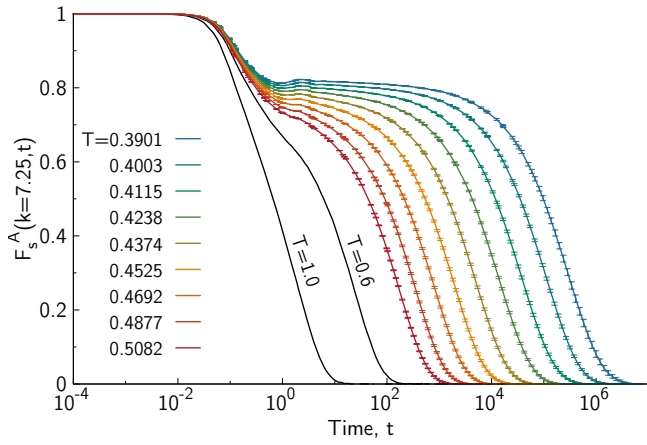


FIG. 2. Self part of the intermediate scattering functions  $F_s^A(k, t)$  obtained from the MD protocol for  $N = 1200$  particles. Errors bars are one standard deviation on the mean, calculated over about 128 runs.

tual collective overlaps

$$Q_c = \frac{1}{N} \sum_{i,j} \Theta(a - |\mathbf{r}_i^\alpha - \mathbf{r}_j^\beta|). \quad (6)$$

A sensible choice of parameter  $a$  is a fraction of the typical interparticle distance. We chose  $a = 0.3$ . We found that both  $Q_s$  and  $Q_c$  are close to the values expected for uncorrelated pairs of configurations, i.e.,  $O(1/N)$  and  $\frac{4}{3}\pi a^3 \rho$ , respectively.

From MD and MC simulations we extract the self part of the intermediate scattering functions

$$F_s^A(k, t) = \langle f_s^A(k, t) \rangle = \left\langle \frac{1}{N_A} \sum_j e^{-i\mathbf{k} \cdot [\mathbf{r}_j(t) - \mathbf{r}_j(0)]} \right\rangle, \quad (7)$$

where the sum runs over the particles of type  $A$ . We choose a wave-vector  $k = 7.25$ , close to the first peak of the structure factor<sup>31</sup>. The corresponding structural relaxation time  $\tau_\alpha$  is defined as usual as  $F_s^A(k, \tau_\alpha) = 1/e$ . In Fig. 2, we show the dynamic data obtained from the MD protocol.

### C. Crystalline order detection

The study of glass-forming liquids is often hampered by crystallization and the very relation between glassy behavior and crystallization remains a matter of debate<sup>46,47</sup>. The KA mixture, which is a simple model of a metallic glass-former, has been extensively used as a model to study the glass transition because of its stability against crystallization. Until very recently, the note added in the proofs of Ref. 48 was, to the best of our knowledge, the only report of crystallization of this model by direct simulation, achieved through runs

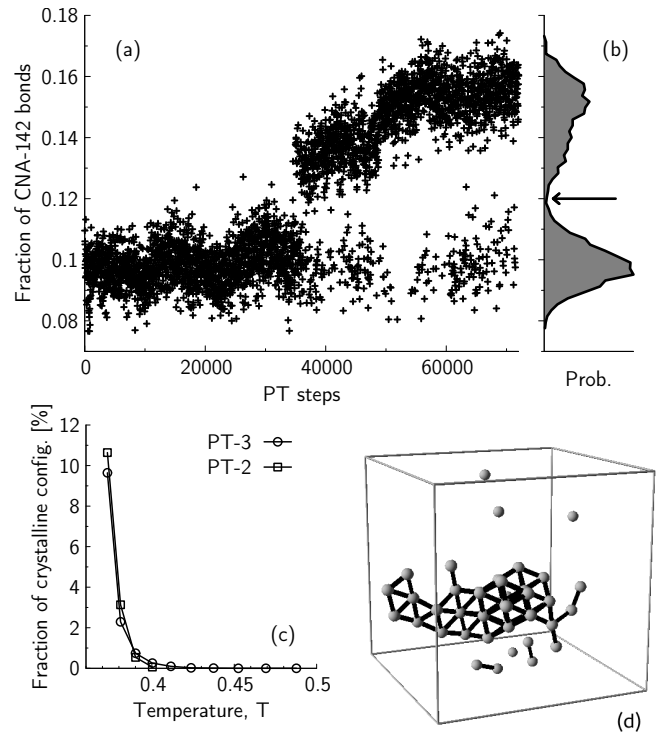


FIG. 3. Detection of crystalline configurations. (a) Crystallization event during a PT-2 simulation for  $N = 1200$  particles. The fraction of CNA-142 bonds,  $f_{142}$ , is shown as a function of PT steps (1 PT step=50000 MD steps). (b) The probability density calculated during the run shows a bimodal distribution with a sharp minimum around  $f_{142} \approx 12\%$ . (c) Percentage of crystalline configurations, detected using a 12% threshold on  $f_{142}$ , as a function of temperature. Below  $T = 0.4$ , both PT-2 and PT-3 protocols have a large fraction of crystalline configurations. PT-2 data were not analyzed above  $T = 0.4$ . (d) Connected component of a cluster formed by particles surrounded by  $A$ -particles only during a crystallization event.

of about  $3.7 \times 10^7$  time units ( $7.4 \times 10^9$  steps) at  $T = 0.40$ . At this temperature, however, the nucleation time is still much larger than the structural relaxation time  $\tau_\alpha$  ( $\sim 10^5$  time units), and therefore MD / MC simulations of the metastable liquid can be carried out safely. In this work, however, we were able to equilibrate the mixture at even lower temperatures. Below  $T = 0.4$ , crystallization events become increasingly frequent, as also demonstrated by a very recent simulation study<sup>49</sup>. Within the studied range of system sizes, the smaller the system, the stronger the tendency to crystallization.

As a first indicator of crystallization events in our simulations, we monitored the evolution of the inherent structure (IS) energy as a function of time<sup>50</sup>. However, the IS energy may also display large but reversible fluctuations, unrelated to crystal nucleation. We thus studied two additional order parameters that allow us to disentangle “amorphous” and crystalline fluctuations. The first one relies on the so-called common neighbor analysis (CNA)<sup>51</sup>. In this approach, the bonds formed by neigh-

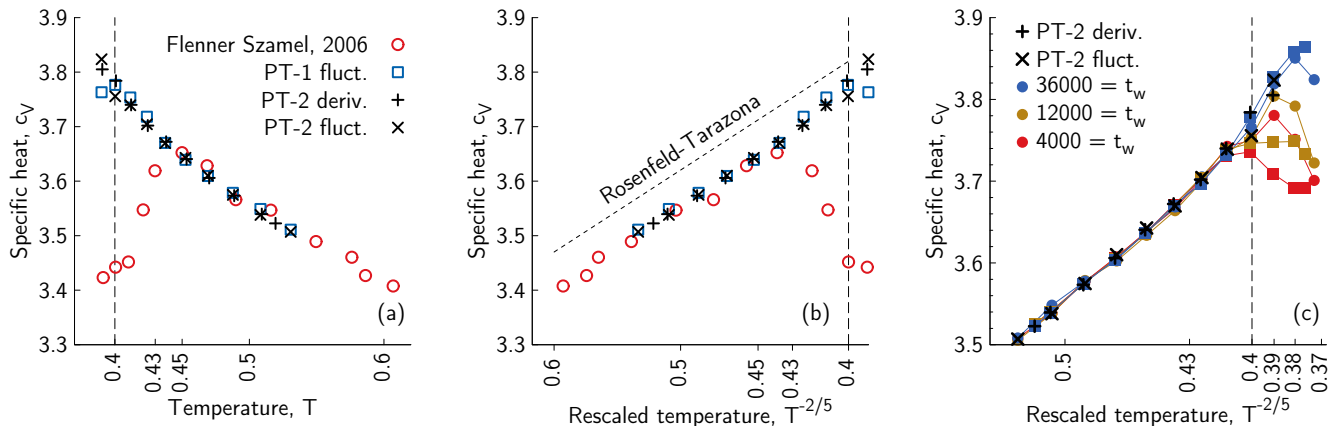


FIG. 4. (a) Specific heat from protocols PT-1 and PT-2 for  $N = 1200$  particles in the regime  $T \gtrsim 0.4$  where crystallization is negligible. Results from fluctuation and derivative expressions of the specific heat are shown as indicated in the legend. The temperature of the data from Ref. 32 (circles) is divided by the density scaling factor  $(1.204/1.2)^\gamma$ , with  $\gamma = 5.0$  to correct for the small density mismatch. (b) Rosenfeld-Tarazona scaling of the same specific heat  $c_V$  data as in panel (a). (c) Specific heat from protocol PT-3 for different waiting times  $t_w$  expressed in unit of PT steps. Results from fluctuation and derivative expressions of the specific heat correspond to circles and squares, respectively. Configurations with  $f_{142} > 0.12$  are discarded from the calculations.

boring particles are classified according to the number of shared neighbors. It has been shown that the fraction  $f_{142}$  of bonds of type 142, see e.g. Ref. 52, allows one to detect crystallization in *biased* simulations of the KA mixture. We found that this approach allows one to detect crystallization in the bulk mixture as well. An example of a crystallization event is depicted in Fig. 3. Even though the nature of the fluctuation is not always clear-cut, we found that a threshold on  $f_{142}$  is an effective criterion to filter out crystalline configurations. Note that since we run several replicas at a time, only a few of them may be affected by crystallization. When this occurs they typically remain “stuck” in the lowest portion of temperature space. As in Ref. 52, we used a threshold of 12% CNA-142 bonds. A large crystalline cluster detected in our simulations is shown in Fig. 3. The crystal nucleus is formed by fcc pockets of  $A$  particles, which implies compositional fluctuations that deplete  $B$  particles. To detect it, we introduced an even simpler order parameter, namely the concentration of cages formed by  $A$  particles only<sup>52</sup>. In particular, we evaluated the connected component<sup>53</sup> of clusters formed by pure- $A$  cages. We found that in typical crystalline samples, the size of these connected clusters is about a few hundred particles. Finally, in Fig.3(c) we show the percentage of crystalline configurations in the simulations of protocol PT-2 and PT-3 for  $N = 1200$  particles. We see that they increase markedly below  $T = 0.4$ . To deal with data analysis in this delicate regime while retaining the maximum possible amount of statistics, we filtered our  $c_V$  measurements by discarding individual configurations whose CNA-142 concentration was higher than 0.12, see Sec. III A. On the other hand, above  $T = 0.4$  the fraction of samples above the crystalline threshold is negligible and we rarely

encountered problematic runs. These runs were simply discarded all together.

### III. RESULTS

#### A. Thermodynamics

The specific heat  $c_V$  is a sensitive, although not unambiguous, indicator of thermodynamic changes in dense liquids. For instance, a sudden drop in  $c_V$  as a function of the control parameters may be due to a phase transition, or more generally to a change in the topography of the underlying energy landscape, but might as well indicate incomplete equilibration, as is the case at the laboratory glass transition observed upon cooling. Previous work on the KA mixture showed the presence of a peak in  $c_V$  at some temperature close to the mode-coupling temperature  $T_{\text{MCT}} = 0.435$ <sup>31</sup>. In this section, we show that the thermodynamics of the KA mixture is regular, i.e., it shows no anomaly, at least down to  $T = 0.39$  and that the peak found in Ref. 32 is due to partial equilibration. Below  $T = 0.4$ , equilibration becomes hard on current simulation time scales and analysis is further hampered by crystallization events. Finally, we discuss the possible presence of a thermodynamic anomaly in this highly metastable portion of the phase diagram.

In Fig. 4(a) we show specific heat measurements from parallel tempering simulations using protocols PT-1 and PT-2. We also include results from a previous study using PT simulations, which reported a peak in  $c_V$  around  $T_{\text{MCT}}$ <sup>32</sup>. From our data, we conclude that no anomaly is observed in the specific heat, which increases monotonically down to  $T = 0.39$ . The length of our simulations

is typically one order of magnitude longer than those of Ref. 32. In retrospect, our work warns that tests such as histogram reweighting or the consistency of fluctuation and derivative expressions of response functions, such as  $c_V$ , are not sufficient to ensure equilibration of supercooled liquids, see Ref. 54 for a more detailed discussion of this issue. Also, our results imply that one needs at least  $\sim 10^9$  MD time steps to equilibrate the KA mixture below  $T_{\text{MCT}}$ .

The empirical model of Rosenfeld-Tarazona<sup>55</sup> proposes the following functional form for the potential energy  $U = aT^{3/5} + b$ , which yields  $c_V \sim T^{-2/5}$ . In Fig. 4(b) we draw the specific heat data from protocols PT-1 and PT-2 as a function of  $T^{-2/5}$ , which linearizes the Rosenfeld-Tarazona law. A similar representation yields an excellent data collapse for simple liquids in both normal and moderately supercooled regime<sup>56</sup>. We find that this functional form provides a very good description of the data but a slight upward bending is observed around  $T = 0.4$ , suggesting the presence of additional fluctuations not accounted for by this simple liquid-state model. This is confirmed by the analysis of the third moment of the potential energy distribution. We found that the skewness remains constant at high temperature and starts to increase slightly around  $T = 0.4$  (not shown), even when crystalline configurations are removed from the analysis. This behavior may be thus attributed to crystallization precursors or to enhanced fluctuations of the locally favored structure of the system<sup>57,58</sup>.

We found that the measurements using PT-1 and PT-2 start to deviate significantly from each other below  $T = 0.39$ . Moreover, in this temperature regime, the liquid has an increased tendency to crystallize, see Sec. II. In Fig. 4(c) we show measurements of  $c_V$  from protocol PT-3, in which crystalline samples are removed on a per-configuration basis and equilibration is assessed directly, i.e., by measuring the waiting time dependence of  $c_V$ . Specifically, we start parallel tempering simulations from previously equilibrated configurations at  $T = 0.4$  and perform averages over restricted portions of the trajectories as follows

$$\langle A \rangle_{t_w} = \frac{1}{t_p - t_x} \int_{t_w}^{t_w+t_p} dt A(t) W(t), \quad (8)$$

where  $t_w$  is the waiting time and  $W(t) = \Theta(0.12 - f_{142})$  is a windowing function that removes from the averages samples identified as crystalline (see Sec. II) and  $t_x = \int_{t_w}^{t_w+t_p} dt (1 - W(t))$ . The production time  $t_p$  was kept fixed to 36000 PT steps, independent of waiting time.

In Fig. 4(c) we show the results obtained by calculating the specific heat starting from time  $t_w$  with increasing values of  $t_w$ . We emphasize that these specific heat measurements cover a temperature regime that has never been probed before at equilibrium. For temperatures higher than 0.4, the results of the PT-3 protocol show a consistent, i.e.,  $t_w$ -independent, growth of  $c_V$ , thus corroborating our previous analysis. Below  $T = 0.4$ ,

the specific heat measurements display a more marked waiting-time dependence but fluctuation and derivative formulas converge for sufficiently long waiting times and reveal a monotonic increase of  $c_V$  down to  $T = 0.38$ . Only at the lowest temperature, the specific heat  $c_V$  measured from energy fluctuations shows a local maximum. The dependence of this peak as a function of waiting time suggests that this feature may be actually due to lack of equilibration.

Recent simulations based on trajectory path sampling<sup>58</sup> suggest the existence of a liquid-liquid transition in the low temperature part of the phase diagram of the KA mixture. Our data narrow down the temperature range over which this hypothetical transition may occur and rule out thermodynamic anomalies for  $T > 0.37$ . These results do not exclude, however, the scenarios discussed in Ref. 58. Given the strong tendency to crystallize below  $T = 0.4$ , however, our results show that a thermodynamic anomaly, if present at all in the KA mixture, is hidden in a highly metastable portion of the phase diagram. In practice, it will be very difficult to detect it in large enough samples. Therefore, we think that future work in this context should focus on more robust models of glass-formers.

## B. Dynamics

The parallel tempering algorithm allows one to accelerate the sampling of static and thermodynamic observables, but it does not provide by itself useful information on the dynamics. However, it is possible to carry out dynamic measurements by using uncorrelated configurations extracted from PT simulations as starting points of conventional molecular dynamics or Monte Carlo simulations. This approach can be parallelized in a trivial way by performing independent simulations and allows one to extend the accessible dynamic range by short-circuiting equilibration issues. In this section, we implement these ideas following using the MD and MC protocols described in Sec. II and test various dynamic crossover scenarios below the MCT temperature.

Figure 5(a) shows an Arrhenius representation of the relaxation times obtained using the MD and MC protocols for 1200 and 3600 particles. We note that equilibrium sampling is ensured by the fact that both MD and MC simulations start from previously equilibrated configurations down to  $T = 0.39$ . The time scale of Monte Carlo simulations has been scaled to match the relaxation times of MD at low temperature. We also include dynamic data from Ref. 57, which agree with the new set of simulations over the common temperature range. Very similar behavior is found also for B-type particles (not shown). Thanks to the hybrid protocols employed in the present work, the accessible dynamic range has increased by almost two orders of magnitude compared to the conventional molecular dynamics simulations of Ref. 57 and we can comfortably study the dynamics be-

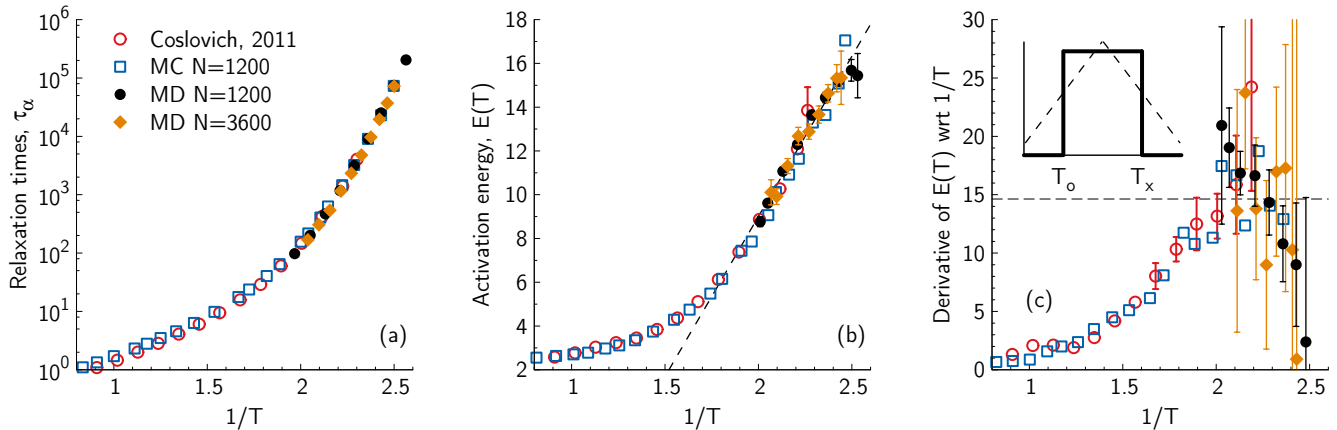


FIG. 5. Temperature-derivative analysis of relaxation times. The relaxation times obtained from MC simulations have been scaled by  $5 \times 10^2$  MC steps. Error bars on MD data represent one standard deviation on the mean and are only shown when larger than the symbol size. (a) Relaxation times  $\tau_\alpha$  as a function of  $1/T$  for various protocols and system sizes. (b) Activation energy  $E(T)$  for the same set of data as panel (a). The dashed line indicates a linear fit to Eq. (11) in the range  $T \leq 0.52$  with  $J = 2.7$  and  $T_0 = 0.72$ . (c) Derivative of  $E(T)$  with respect to  $1/T$ . The horizontal line corresponds to  $2J^2$ . The inset shows a schematic representation of two possible scenarios for this derivative: the solid line depicts the behavior expected from facilitation models, while the dashed line is the qualitative behavior described in Ref. 21.

low  $T_{\text{MCT}}$ . The data suggest that the temperature dependence of the relaxation times gets milder, i.e., more Arrhenius-like, at the lowest temperatures. However, it is notoriously difficult to draw firm conclusions based on analysis of the relaxation time alone, which has led to a number of controversies<sup>12</sup>.

Temperature-derivative analysis of the dynamic data provides a most stringent test of analytic expressions for  $\tau_\alpha(T)$  and is particularly well-suited to reveal the presence of a dynamic crossover<sup>19–21</sup>. Even though this approach requires very accurate data, it has the advantage of being parameter free and requires no data fitting. So far, it has mostly been applied to high-quality dielectric relaxation measurements. To the best of our knowledge, the only numerical study to conduct this analysis across the MCT temperature is Ref. 59 for a mixtures of harmonic spheres. Here, we push this kind of analysis even further by combining the trivial parallelism of our MD and MC protocols and the efficiency of the RUMD simulation package on small system sizes<sup>41</sup>.

The central quantity in our analysis is the apparent activation energy

$$E(T) = \frac{d \ln \tau_\alpha}{d(1/T)}, \quad (9)$$

which we compute by the centered difference method<sup>60</sup>. A graph of  $E(T)$  versus  $1/T$  provides a simple way to test the parabolic law proposed by Elmatald et al.<sup>22</sup> in the context of dynamic facilitation

$$\tau_\alpha = \tau_0 \exp \left[ \left( \frac{J}{T_0} \right)^2 \left( \frac{T_0}{T} - 1 \right)^2 \right], \quad (10)$$

where  $\tau_0$ ,  $J$ , and  $T_0$  are material parameters. The activation energy is then a linear function of  $1/T$  given by

the following expression

$$E_p(T) = \frac{2J^2}{T_0} (T_0/T - 1). \quad (11)$$

It should be emphasized that Eq. (10) is only expected to hold below the onset temperature  $T_0$  and above an additional reference temperature  $T_x$ . Outside this range of temperatures, the dynamics is expected to be Arrhenius<sup>22</sup>.

A similar approach can be used to linearize the classic VFT equation. Following Stickel et al.<sup>19</sup> we introduce  $\phi = E(T)^{-1/2}$ . By computing the derivative of the VFT expression

$$\tau_\alpha = \tau_0 \exp \left[ \frac{T_{\text{vft}}}{K(T - T_{\text{vft}})} \right], \quad (12)$$

we obtain

$$\phi(T) = \sqrt{\frac{K}{T_{\text{vft}}}} \left( 1 - \frac{T_{\text{vft}}}{T} \right), \quad (13)$$

where  $\tau_0$ ,  $K$ , and  $T_{\text{vft}}$  are parameters. Thus, the VFT equation appears linear in a graph where  $\phi$  is shown as a function of  $1/T$ <sup>19</sup>.

In Fig. 5(b) we show  $E(T)$  as a function of  $1/T$ . Overall, the activation energy displays an approximately linear behavior at sufficiently low temperature, i.e.,  $T < 0.5$ . This behavior is well captured by Eq. (11), although fitting the relaxation times in this range requires a value  $T_0 \approx 0.72$ , which is lower than the usual estimates  $0.8 - 1.0$ , see e.g. Ref. 61, but consistent with a very recent analysis<sup>62</sup> based on Eq. (11). We also note that the value of  $J/T_0 = 3.7$  is larger than the one used in Ref. 22.



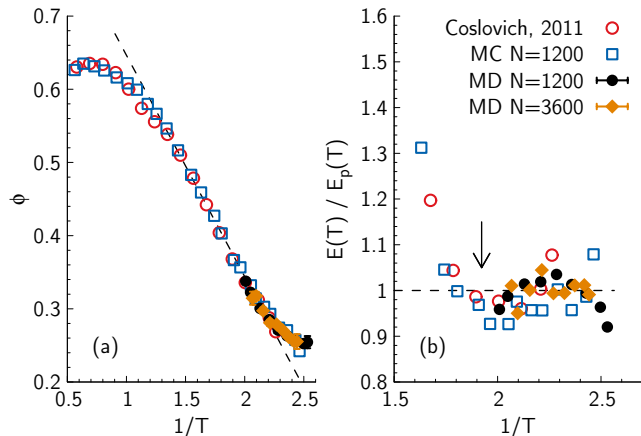


FIG. 6. Critical assessment of the VFT and parabolic laws. (a) Stickel plot  $\phi(T)$  versus  $1/T$ . (b) Plot of  $E(T)/E_p(T)$  as a function of  $1/T$ . The dashed lines are guides to the eye. The arrow indicates the temperature  $T = 0.52$  from which the parabolic law begins to apply.

The fit parameters used in Ref. 22 appear to strike a balance between the high and low  $T$  portions of the data. For the most accurate data set, i.e., MD with  $N = 1200$ , and at the lowest temperatures, this representation also reveals a slight inflection in  $E(T)$ . This slight saturation may suggest a dynamic crossover similar to the one observed in certain molecular glass-formers<sup>63</sup> and in the simulation of harmonic spheres<sup>59</sup>. One comment on possible finite size effects is in order. In a small sample, the activation energy necessarily reaches an upper bound and a smooth crossover to Arrhenius behavior is expected at a system-size dependent temperature<sup>64</sup>. Within the quality of our data the temperature dependence for different system sizes gives compatibles results. However, due to the larger scatter in the  $N = 3600$  samples, we cannot completely rule out the possibility that the inflection of the  $N = 1200$  is due to a finite size effect.

Pushing our analysis one step further, we compute the derivative of  $E(T)$  with respect to  $1/T$  and show the results in Fig. 5(c). This quantity should be constant and equal to  $2J^2$  in the dynamic facilitation scenario, whereas other models<sup>63</sup> predict that it should peak around some crossover temperature. The inset of the figure illustrates schematically these two possible scenarios. Within the noise of the data, and in particular of our most accurate data set (MD with  $N = 1200$ ), our measurements are compatible with a decrease of  $dE(T)/d(1/T)$  below some temperature  $T_D$  close to  $T_{MCT}$ . Simulations at even lower temperature and better statistics for larger system sizes would be needed to fully confirm this behavior.

In Fig. 6(a) we test the validity of the VFT law by computing  $\phi(T)$  as a function of  $1/T$ . We find that the VFT law holds well at intermediate temperatures, but clear deviations are visible at low temperature. This confirms the well-known observation<sup>19</sup> that, except in rare cases, the VFT equation cannot describe the full  $T$  de-

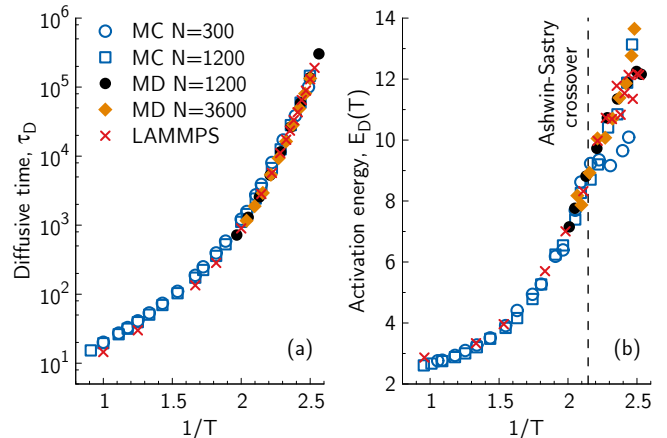


FIG. 7. Analysis of diffusive times  $\tau_D$ . The diffusive times obtained from MC simulations have been scaled by  $5 \times 10^2$  MC steps. (a) Arrhenius representation of the diffusive times  $\tau_D$ . (b) Activation energies from the diffusive time  $\tau_D$ . The vertical line indicates the crossover observed by Ashwin and Sastry in Ref. 33 for a system of 256 particles.

pendence of the dynamic data. In Fig. 6(b) we show a plot  $E(T)/E_p(T)$  vs  $1/T$ . In this representation, the parabolic law would correspond to a horizontal line. We see that the data flatten out only below  $T = 0.52$ , thus the range over which this law holds in the KA mixture is actually more limited than previously thought<sup>22</sup>.

We also computed the activation energy  $E_D$  from the diffusive time  $\tau_D$ , defined as the time needed to reach a mean square displacement of A particles equal to 1. These diffusive times are shown in Fig. 7(a) for several protocols and system sizes. We then compute, as before, the activation energies  $E_D$  associated to diffusive times  $\tau_D$ . Figure 7(b) indicates that the growth of  $E_D$  gets milder below some crossover temperature  $T_D \simeq 0.45$ . Again, our  $N = 1200$  MD data-set suggests an inflection of  $E_D$  around this temperature. This crossover temperature is remarkably close to the one reported long ago by Ashwin and Sastry in Ref. 33 for a smaller system size ( $N = 256$ ). However, in small systems  $E_D$  actually saturates at  $T_D$ , while bigger samples only cross over to a milder temperature dependence. These results indicate that, even though the results of Ref. 33 were probably affected by finite size effects, the diffusion mechanism might actually change in a temperature range close to the MCT transition temperature. This is corroborated by the analysis of a much larger sample ( $N = 100000$ ) simulated using LAMMPS, which gives a trend compatible with the ones observed for  $N = 1200$  and  $N = 3600$  particles. These large-scale simulations were performed in the  $NVT$  simulations using the Nose-Hoover thermostat but without parallel tempering.

Finally, we compute the dynamic fluctuations associ-

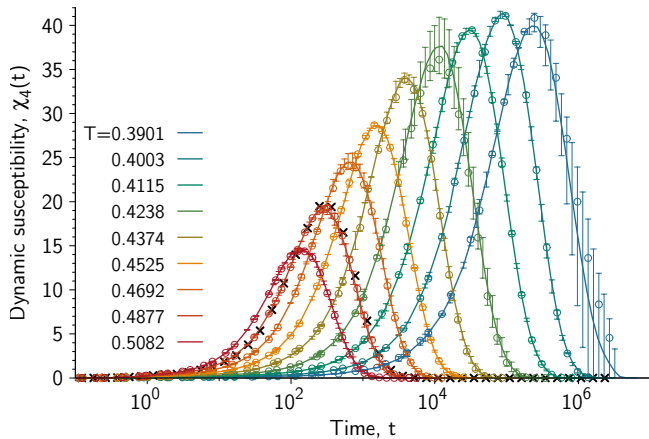


FIG. 8. Dynamic susceptibility  $\chi_4(t)$  from MD protocol (*NVT* ensemble) for  $N = 1200$  particles. The full lines are measurements over the entire length of the runs, while the symbols are measurements restricted to the first half of the runs. The error bars are estimated from the difference between the first and second halves of the runs. The crosses correspond to  $\chi_4^{NVE}(t) + T^2 \left( \frac{dQ_s}{dT}(t) \right)^2 / c_V$ , see Eq. (16), at  $T = 0.4877$ .

ated to the time-dependent self overlap function

$$Q_s(t) = N^{-1} \sum_j \Theta(0.3 - |\mathbf{r}_j(t) - \mathbf{r}_j(0)|), \quad (14)$$

where the sum is taken over all particles. The dynamic susceptibility is then defined as

$$\chi_4(t) = N \{ \langle [Q_s(t)^2] \rangle - \langle Q_s(t) \rangle^2 \}, \quad (15)$$

where [...] indicates an average over statistically independent initial samples and  $\langle \dots \rangle$  a time average over a given run. The dynamic susceptibilities, shown in Fig. 8 for  $N = 1200$ , display a peak at a time  $\tau_4$  proportional to the structural relaxation time. The peak height  $\chi_4^*$  is a standard proxy for the extent of dynamic heterogeneity in supercooled liquids<sup>3</sup>.

In Figs. 9(a) and (b) we show  $\chi_4^*$  as a function of  $1/T$  and as a function of  $\tau_4^*$ , respectively. The dynamic fluctuations quantified by the susceptibility in the *NVT* ensemble cross over around the MCT temperature to a very mild dependence on both temperature and relaxation time. Within the quality of our data, this effect *cannot* be attributed to the finite size of the system. We point out, however, that the MCT scaling expected in the *NVT* ensemble<sup>65</sup>,  $\chi_4^* \sim \tau_\alpha^{\gamma/2} \sim \tau_4^{\gamma/2}$ , where  $\gamma \approx 2.4$  is the exponent of power law fit to the relaxation time, does not hold well for this system. Therefore, the fact that the crossover in the dynamic susceptibility occurs close to the mode-coupling temperature may be coincidental. We also note that similar results may not hold for the full dynamic susceptibility<sup>3</sup>, which includes contributions from number and concentration fluctuations and which we have neglected here. Our results resonate with

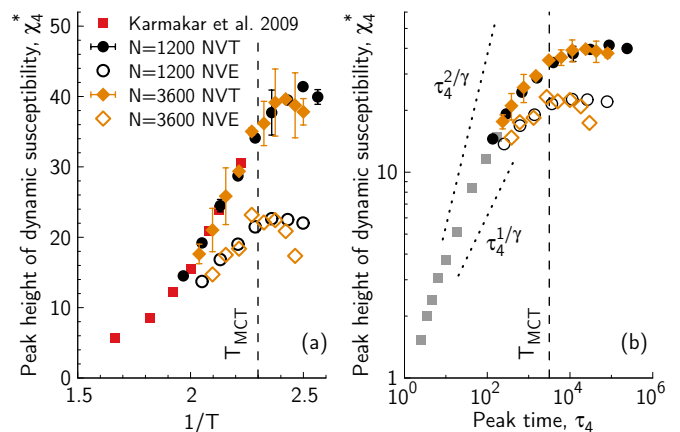


FIG. 9. Peak height of the dynamic susceptibility  $\chi_4^*$  in the *NVT* ensemble (full symbols) and in the *NVE* ensemble (empty symbols) as a function of (a)  $1/T$  and (b) the peak time  $\tau_4$ . The vertical line in the two panels marks the MCT temperature. The dotted lines in panel (b) indicate the predicted MCT scaling in the *NVT* (exponent  $2/\gamma$ ) and *NVE* ensemble (exponent  $1/\gamma$ ). Squares in panel (a) are taken from Ref. 69. Squares in panel (b) indicate results from additional, high temperature *NVT* simulations for  $N = 1200$  particles.

those of Flenner and Szamel<sup>66</sup>, who showed that some contributions to the total susceptibility, notably those associated to dynamic fluctuations in the *NVE* ensemble, may be more sensitive to the presence of a crossover than the full susceptibility. To address this point quantitatively, we computed the dynamic susceptibility in the *NVE* ensemble from the exact expression<sup>67</sup>

$$\chi_4^{NVE}(t) = \chi_4^{NVT}(t) - \frac{T^2}{c_V} \left( \frac{dQ_s}{dT}(t) \right)^2. \quad (16)$$

We checked that the above expression yields results consistent with those obtained from simulations in the *NVE* ensemble at  $T = 0.4877$ , at which the energy drift during *NVE* simulations was not too severe, see Fig. 8. The temperature dependence of the peak height of  $\chi_4^{NVE}(t)$ , shown in Fig. 9, provides clear hints of a dynamic crossover around the MCT temperature and corroborates the findings of Ref. 66. Royall et al.<sup>68</sup> have also noted that the growth of  $\chi_4^*$  observed in simulations at above  $T_{MCT}$  is incompatible with the typical correlation lengths measured experimentally. From this point of view, our finding of a crossover to a much milder rate of growth of dynamic correlations is a welcome result, which may solve the apparent conundrum evidenced in Ref. 68.

#### IV. CONCLUSIONS

In this work we have performed extensive computer simulations to probe the existence of thermodynamic and

dynamic anomalies in the Kob-Andersen binary Lennard-Jones mixture. Our simulations build on an efficient simulation setup, which combines algorithmic and hardware optimizations. In particular, we exploit the parallel tempering algorithm and multi-GPU acceleration to measure the specific heat at equilibrium down to unprecedented temperatures. We also appreciably extend the range of dynamic measurements by starting regular MD and MC simulations from independent configurations previously equilibrated with parallel tempering. This approach is trivially parallel and enables us to perform a temperature-derivative analysis of the dynamic data.

Thanks to these advances, we could clarify some issues related to the thermodynamic and dynamic behavior of the mixture. In particular, we found that the specific heat increases monotonically down to at least  $T = 0.38$ , in contrast with previous findings<sup>32</sup>, which suggested a maximum around  $T = 0.43$  and which was probably due to out-of-equilibrium effects. Although crystallization renders the analysis difficult at low temperature, our data indicate that thermodynamic anomalies, if present at all, must occur in a highly metastable, low-temperature portion of the phase diagram. Conversely, any possible crossover above  $T = 0.38$  must be purely dynamic in origin. By performing a temperature-derivative analysis of the dynamic data and by analyzing the dynamic susceptibilities, we have assessed several scenarios that may involve a dynamic crossover in this temperature regime. One possible scenario suggests the presence of a crossover<sup>27,30</sup> around the mode-coupling temperature  $T_{MCT}$ . There are however alternative interpretations that attribute the dynamic crossover to a saturation of energy barriers, as is the case in elastic models<sup>70,71</sup>, free-volume models<sup>72</sup> and even possibly in the dynamic facilitation scenario at sufficiently low temperature<sup>73</sup>. In these latter scenarios, the crossover need not be around  $T_{MCT}$ .

Although our analysis is not entirely conclusive yet, we argue that state-of-the-art simulation methods combined with temperature-derivative analysis of simulation data may hold the key to fully disentangle these scenarios in the near future. Judging from the quality of our temperature-derivative analysis and dynamic fluctuations measurements, we infer that simulations of the order of several thousands of structural relaxation times are needed to fully confirm or rule out the presence of dynamic crossovers. Our results also suggest that contributions to the dynamic susceptibility measured in ensembles where conserved quantities are not free to fluctuate may better probe the dynamic behavior than the full susceptibility<sup>65</sup>. For specific systems, specialized Monte Carlo moves, like particle swaps<sup>74–78</sup>, may provide an additional and important efficiency improvement and facilitate thermodynamic and dynamic studies below the mode-coupling temperature.

## ACKNOWLEDGMENTS

We thank E. Flenner and G. Szamel for useful discussions. We acknowledge PRACE for awarding us access to Curie at GENCI@CEA, France, which enabled the development of part of the software used in this work. Data relevant to this work can be accessed at <https://doi.org/10.5281/zenodo.1227831>.

The final publication is available at Springer via <http://dx.doi.org/10.1140/epje/i2018-11671-2>, albeit with bitmapped figures.

## AUTHOR CONTRIBUTION STATEMENT

The simulations were performed as follows: protocol PT-1 and LAMMPS by WK, protocol PT-2, PT-3, and MD by DC and MC by MO. DC and MO analyzed the data. DC wrote the first draft of the article. All authors discussed the results and contributed to the final manuscript.

- <sup>1</sup>C. A. Angell *et al.*, “Formation of glasses from liquids and biopolymers,” *Science* **267**, 1924 (1995).
- <sup>2</sup>K. Binder and W. Kob, *Glassy materials and disordered solids: An introduction to their statistical mechanics* (World Scientific, 2011).
- <sup>3</sup>L. Berthier and G. Biroli, “Theoretical perspective on the glass transition and amorphous materials,” *Rev. Mod. Phys.* **83**, 587 (2011).
- <sup>4</sup>C. A. Angell, “Glass-formers and viscous liquid slowdown since David Turnbull: Enduring puzzles and new twists,” *MRS Bull.* **33**, 544 (2008).
- <sup>5</sup>P. Scheidler, W. Kob, A. Latz, J. Horbach, and K. Binder, “Frequency-dependent specific heat of viscous silica,” *Phys. Rev. B* **63**, 104204 (2001).
- <sup>6</sup>I. Saika-Voivod, F. Sciortino, and P. H. Poole, “Free energy and configurational entropy of liquid silica: Fragile-to-strong crossover and polyamorphism,” *Phys. Rev. E* **69**, 041503 (2004).
- <sup>7</sup>S. Saito, I. Ohmine, and B. Bagchi, “Frequency dependence of specific heat in supercooled liquid water and emergence of correlated dynamics,” *J. Chem. Phys.* **138**, 094503 (2013).
- <sup>8</sup>A. J. Moreno, S. V. Buldyrev, E. La Nave, I. Saika-Voivod, F. Sciortino, P. Tartaglia, and E. Zaccarelli, “Energy Landscape of a Simple Model for Strong Liquids,” *Phys. Rev. Lett.* **95**, 157802 (2005).
- <sup>9</sup>L. Xu, S. V. Buldyrev, N. Giovambattista, C. A. Angell, and H. E. Stanley, “A monatomic system with a liquid-liquid critical point and two distinct glassy states,” *J. Chem. Phys.* **130**, 054505 (2009).
- <sup>10</sup>R. Gutiérrez, S. Karmakar, Y. G. Pollack, and I. Procaccia, “The static lengthscale characterizing the glass transition at lower temperatures,” *EPL* **111**, 56009 (2015).
- <sup>11</sup>M. Ozawa, K. Kim, and K. Miyazaki, “Tuning pairwise potential can control the fragility of glass-forming liquids: from a tetrahedral network to isotropic soft sphere models,” *J. Stat. Mech. Theory Exp.* **2016**, 074002 (2016).
- <sup>12</sup>F. Mallamace, C. Branca, C. Corsaro, N. Leone, J. Spooren, S.-H. Chen, and H. E. Stanley, “Transport properties of glass-forming liquids suggest that dynamic crossover temperature is as important as the glass transition temperature,” *Proc. Natl. Acad. Sci. USA* **107**, 22457 (2010).
- <sup>13</sup>C. Zhang, L. Hu, Y. Yue, and J. C. Mauro, “Fragile-to-strong transition in metallic glass-forming liquids,” *J. Chem. Phys.* **133**, 014508 (2010).

- <sup>14</sup>C. Zhou, L. Hu, Q. Sun, H. Zheng, C. Zhang, and Y. Yue, “Structural evolution during fragile-to-strong transition in *cuzr* (al) glass-forming liquids,” *J. Chem. Phys.* **142**, 064508 (2015).
- <sup>15</sup>K. N. Lad, N. Jakse, and A. Pasturel, “Signatures of fragile-to-strong transition in a binary metallic glass-forming liquid,” *J. Chem. Phys.* **136**, 104509 (2012).
- <sup>16</sup>S. Wei, F. Yang, J. Bednarcik, I. Kaban, O. Shuleshova, A. Meyer, and R. Busch, “Liquid–liquid transition in a strong bulk metallic glass-forming liquid,” *Nat. Commun.* **4** (2013), 10.1038/ncomms3083.
- <sup>17</sup>M. Stolpe, I. Jonas, S. Wei, Z. Evenson, W. Hembree, F. Yang, A. Meyer, and R. Busch, “Structural changes during a liquid-liquid transition in the deeply undercooled  $Zr_{58.5}Cu_{15.6}Ni_{12.8}Al_{10.3}Nb_{2.8}$  bulk metallic glass forming melt,” *Phys. Rev. B* **93**, 014201 (2016).
- <sup>18</sup>X. Yang, C. Zhou, Q. Sun, L. Hu, J. C. Mauro, C. Wang, and Y. Yue, “Anomalous crystallization as a signature of the fragile-to-strong transition in metallic glass-forming liquids,” *J. Phys. Chem. B* **118**, 10258 (2014).
- <sup>19</sup>F. Stickel, E. W. Fischer, and R. Richert, “Dynamics of glass-forming liquids. I. Temperature-derivative analysis of dielectric relaxation data,” *J. Chem. Phys.* **102**, 6251 (1995).
- <sup>20</sup>J. C. Martinez-Garcia, J. Martinez-Garcia, S. J. Rzoska, and J. Hulliger, “The new insight into dynamic crossover in glass forming liquids from the apparent enthalpy analysis,” *J. Chem. Phys.* **137**, 064501 (2012).
- <sup>21</sup>V. N. Novikov and A. P. Sokolov, “Qualitative change in structural dynamics of some glass-forming systems,” *Phys. Rev. E* **92** (2015), 10.1103/PhysRevE.92.062304, 1510.05529.
- <sup>22</sup>Y. S. Elmatad, D. Chandler, and J. P. Garrahan, “Corresponding States of Structural Glass Formers,” *J. Phys. Chem. B* **113**, 5563 (2009), 0811.2450.
- <sup>23</sup>R. Casalini, M. Paluch, and C. M. Roland, “Dynamic crossover in supercooled liquids induced by high pressure,” *J. Chem. Phys.* **118**, 5701 (2003).
- <sup>24</sup>R. Casalini and C. M. Roland, “Viscosity at the Dynamic Crossover in *o*-Terphenyl and Salol under High Pressure,” *Phys. Rev. Lett.* **92**, 245702 (2004).
- <sup>25</sup>W. Götze, *Complex dynamics of glass-forming liquids: A mode-coupling theory* (Oxford University Press, 2008).
- <sup>26</sup>W. Kob, S. Roldán-Vargas, and L. Berthier, “Non-monotonic temperature evolution of dynamic correlations in glass-forming liquids,” *Nat. Phys.* **8**, 164 (2012).
- <sup>27</sup>L. Berthier, G. Biroli, D. Coslovich, W. Kob, and C. Toninelli, “Finite-size effects in the dynamics of glass-forming liquids,” *Phys. Rev. E* **86**, 031502 (2012).
- <sup>28</sup>G. Biroli and J. Bouchaud, “The random firstorder transition theory of glasses: A critical assessment,” in *Structural Glasses and Supercooled Liquids* (Wiley-Blackwell, 2012) Chap. 2, p. 31.
- <sup>29</sup>T. Rizzo and T. Voigtmann, “Qualitative features at the glass crossover,” *EPL* **111**, 56008 (2015).
- <sup>30</sup>T. Rizzo, “Dynamical Landau theory of the glass crossover,” *Phys. Rev. B* **94**, 014202 (2016).
- <sup>31</sup>W. Kob and H. C. Andersen, “Testing mode-coupling theory for a supercooled binary Lennard-Jones mixture I: The van Hove correlation function,” *Phys. Rev. E* **51**, 4626 (1995).
- <sup>32</sup>E. Flenner and G. Szamel, “Hybrid Monte Carlo simulation of a glass-forming binary mixture,” *Phys. Rev. E* **73**, 061505 (2006).
- <sup>33</sup>S. S. Ashwin and S. Sastry, “Low-temperature behaviour of the Kob–Andersen binary mixture,” *J. Phys.: Condens. Matter* **15**, S1253 (2003).
- <sup>34</sup>B. Doliwa and A. Heuer, “Energy barriers and activated dynamics in a supercooled Lennard-Jones liquid,” *Phys. Rev. E* **67**, 031506 (2003).
- <sup>35</sup>K. Hukushima and K. Nemoto, “Exchange Monte Carlo method and application to spin glass simulations,” *J. Phys. Soc. Jpn.* **65**, 1604 (1996).
- <sup>36</sup>S. Plimpton, “Fast parallel algorithms for short-range molecular dynamics,” *J. Comp. Phys.* **117**, 1 (1995).
- <sup>37</sup>“LAMMPS: Large-scale Atomic/Molecular Massively Parallel Simulator,” <http://lammps.sandia.gov/>.
- <sup>38</sup>R. Yamamoto and W. Kob, “Replica-exchange molecular dynamics simulation for supercooled liquids,” *Phys. Rev. E* **61**, 5473 (2000).
- <sup>39</sup>D. Frenkel and B. Smit, *Understanding molecular simulation: from algorithms to applications*, Vol. 1 (Academic press, 2001).
- <sup>40</sup>“atooms-pt: Multi-core / multi-GPU parallel tempering,” <https://doi.org/10.5281/zenodo.1183663> ().
- <sup>41</sup>N. Bailey, J. S. Hansen, T. Ingebrigtsen, A. Veldhorst, L. Bohling, C. Lemarchand, A. Olsen, A. Bacher, L. Costigliola, U. Pedersen, and et al., “RUMD: A general purpose molecular dynamics package optimized to utilize GPU hardware down to a few thousand particles,” *SciPost Physics* **3**, 038 (2017).
- <sup>42</sup>“atooms: A python framework for simulations of interacting particles,” <https://doi.org/10.5281/zenodo.1183301> ().
- <sup>43</sup>“mpi4py,” <http://mpi4py.scipy.org/docs/>.
- <sup>44</sup>L. Berthier and W. Kob, “The Monte Carlo dynamics of a binary Lennard-Jones glass-forming mixture,” *J. Phys. Condens. Matter* **19**, 205130 (2007).
- <sup>45</sup>C. Donati, S. Franz, S. C. Glotzer, and G. Parisi, “Theory of non-linear susceptibility and correlation length in glasses and liquids,” *J. Non-Cryst. Solids* **307**, 215 (2002).
- <sup>46</sup>T. Kawasaki and H. Tanaka, “Formation of a crystal nucleus from liquid,” *Proc. Natl. Acad. Sci. USA* **107**, 14036 (2010).
- <sup>47</sup>H. Tanaka, “Bond orientational order in liquids: Towards a unified description of water-like anomalies, liquid-liquid transition, glass transition, and crystallization,” *Eur. Phys. J. E* **35**, 1 (2012).
- <sup>48</sup>S. Toxvaerd, U. R. Pedersen, T. B. Schroder, and J. C. Dyre, “Stability of supercooled binary liquid mixtures,” *J. Chem. Phys.* **130**, 224501 (2009).
- <sup>49</sup>T. S. Ingebrigtsen, J. C. Dyre, T. B. Schrder, and C. P. Royall, “Crystallisation instability in glassforming mixtures,” [arXiv:1804.01378](https://arxiv.org/abs/1804.01378) (2018).
- <sup>50</sup>F. H. Stillinger and T. A. Weber, “Hidden structure in liquids,” *Phys. Rev. A* **25**, 978 (1982).
- <sup>51</sup>J. D. Honeycutt and H. C. Andersen, “Molecular dynamics study of melting and freezing of small Lennard-Jones clusters,” *J. Phys. Chem.* **91**, 4950 (1987).
- <sup>52</sup>L. O. Hedges, R. L. Jack, J. P. Garrahan, and D. Chandler, “Dynamic Order-Disorder in Atomistic Models of Structural Glass Formers,” *Science* **323**, 1309 (2009).
- <sup>53</sup>M. Newman, *Networks: An Introduction*, 1st ed. (Oxford University Press, Oxford ; New York, 2010).
- <sup>54</sup>G. Odriozola and L. Berthier, “Equilibrium equation of state of a hard sphere binary mixture at very large densities using replica exchange Monte Carlo simulations,” *J. Chem. Phys.* **134**, 054504 (2011).
- <sup>55</sup>Y. Rosenfeld and P. Tarazona, “Density functional theory and the asymptotic high density expansion of the free energy of classical solids and fluids,” *Mol. Phys.* **95**, 141?150 (1998).
- <sup>56</sup>T. S. Ingebrigtsen, A. A. Veldhorst, T. B. Schroder, and J. C. Dyre, “Communication: The rosenfeld-tarazona expression for liquids specific heat: A numerical investigation of eighteen systems,” *J. Chem. Phys.* **139**, 171101 (2013).
- <sup>57</sup>D. Coslovich, “Locally preferred structures and many-body static correlations in viscous liquids,” *Phys. Rev. E* **83**, 051505 (2011).
- <sup>58</sup>F. Turci, C. P. Royall, and T. Speck, “Nonequilibrium phase transition in an atomistic glassformer: The connection to thermodynamics,” *Phys. Rev. X* **7**, 031028 (2017).
- <sup>59</sup>W. Kob and D. Coslovich, “Nonlinear dynamic response of glass-forming liquids to random pinning,” *Phys. Rev. E* **90**, 052305 (2014).
- <sup>60</sup>Given a set  $\{x_i\}$  of points and corresponding function values  $\{f_i\}$ , with  $0 \leq i \leq M$ , we compute the derivative at  $(x[i+1]+x[i-1])/2$  as  $(f[i+1] - f[i-1])/(x[i+1] - x[i-1])$  if  $0 < i < M$ . We use  $(f[1] - f[0])/(x[1] - x[0])$  and  $(f[M] - f[M-1])/(x[M] - x[M-1])$  for the first and last pairs of points, respectively. The expression used at the boundaries is more noisy than the one for  $0 < i < M$ .

- <sup>61</sup>S. Sastry, P. G. Debenedetti, and F. H. Stillinger, “Signatures of distinct dynamical regimes in the energy landscape of a glass-forming liquid,” *Nature* **393**, 554 (1998).
- <sup>62</sup>A. Hudson and K. K. Mandadapu, “On the nature of the glass transition in atomistic models of glass formers,” [arXiv:1804.03769](https://arxiv.org/abs/1804.03769) (2018).
- <sup>63</sup>V. N. Novikov and A. P. Sokolov, “Universality of the dynamic crossover in glass-forming liquids: A “magic” relaxation time,” *Phys. Rev. E* **67**, 031507 (2003).
- <sup>64</sup>K. Kim and R. Yamamoto, “Apparent finite-size effects in the dynamics of supercooled liquids,” *Phys. Rev. E* **61**, R41 (2000).
- <sup>65</sup>L. Berthier, G. Biroli, J.-P. Bouchaud, W. Kob, K. Miyazaki, and D. R. Reichman, “Spontaneous and induced dynamic correlations in glass formers. II. Model calculations and comparison to numerical simulations,” *J. Chem. Phys.* **126**, 184504 (2007).
- <sup>66</sup>E. Fleener and G. Szamel, “Dynamic heterogeneities above and below the mode-coupling temperature: Evidence of a dynamic crossover,” *J. Chem. Phys.* **138**, 12A523 (2013).
- <sup>67</sup>L. Berthier, G. Biroli, J.-P. Bouchaud, W. Kob, K. Miyazaki, and D. R. Reichman, “Spontaneous and induced dynamic fluctuations in glass formers. I. General results and dependence on ensemble and dynamics,” *J. Chem. Phys.* **126**, 184503 (2007).
- <sup>68</sup>C. P. Royall, A. Malins, A. J. Dunleavy, and R. Pinney, “Strong geometric frustration in model glassformers,” *J. Non-Cryst. Solids* **407**, 34 (2015).
- <sup>69</sup>S. Karmakar, C. Dasgupta, and S. Sastry, “Growing length and time scales in glass-forming liquids,” *Proc. Natl. Acad. Sci. USA* **106**, 3675 (2009).
- <sup>70</sup>J. C. Dyre, “Colloquium: The glass transition and elastic models of glass-forming liquids,” *Rev. Mod. Phys.* **78**, 953 (2006).
- <sup>71</sup>S. Mirigian and K. S. Schweizer, “Elastically cooperative activated barrier hopping theory of relaxation in viscous fluids. i. general formulation and application to hard sphere fluids,” *J. Chem. Phys.* **140**, 194506 (2014).
- <sup>72</sup>M. H. Cohen and G. S. Grest, “Liquid-glass transition, a free-volume approach,” *Phys. Rev. B* **20**, 1077 (1979).
- <sup>73</sup>Y. S. Elmatad, D. Chandler, and J. P. Garrahan, “Corresponding States of Structural Glass Formers. II,” *J. Phys. Chem. B* **114**, 17113 (2010).
- <sup>74</sup>D. Gazzillo and G. Pastore, “Equation of state for symmetric non-additive hard-sphere fluids: An approximate analytic expression and new Monte Carlo results,” *Chem. Phys. Lett.* **159**, 388 (1989).
- <sup>75</sup>P. Sindzingre, C. Massobrio, G. Ciccotti, and D. Frenkel, “Calculation of partial enthalpies of an argon-krypton mixture by NPT molecular dynamics,” *Chem. Phys.* **129**, 213 (1989).
- <sup>76</sup>T. S. Grigera and G. Parisi, “Fast Monte Carlo algorithm for supercooled soft spheres,” *Phys. Rev. E* **63**, 045102 (2001).
- <sup>77</sup>A. Ninarello, L. Berthier, and D. Coslovich, “Models and algorithms for the next generation of glass transition studies,” *Phys. Rev. X* **7**, 021039 (2017).
- <sup>78</sup>L. Berthier, D. Coslovich, A. Ninarello, and M. Ozawa, “Equilibrium sampling of hard spheres up to the jamming density and beyond,” *Phys. Rev. Lett.* **116**, 238002 (2016).